

Evidence for the Alternating Next-Nearest Neighbor model in the dynamic behavior of a frustrated antiferromagnet

Adra Carr,^{1,2,*} John Bowlan,^{3,*} Claudio Mazzoli,⁴ Andi Barbour,⁴ Wen Hu,⁴ Stuart Wilkins,⁴ Colby Walker,^{1,5} Xiaxin Ding,^{2,†} Jong Hyuk Kim,⁶ Nara Lee,⁶ Young Jai Choi,⁶ Shi-Zeng Lin,⁷ Richard L. Sandberg,^{1,5} and Vivien S. Zapf²

¹Center for Integrated Nanotechnologies, Los Alamos National Laboratory, Los Alamos, New Mexico 87545, USA

²National High Magnetic Field Laboratory, Los Alamos National Laboratory, Los Alamos, New Mexico 87545, USA

³C-PCS, Los Alamos National Laboratory, Los Alamos, NM 87545

⁴NSLS-II Brookhaven National Laboratory, Upton, New York, USA

⁵Department of Physics and Astronomy, Brigham Young University, Provo, Utah, 84602

⁶Dept of Physics, Yonsei University, Seoul 03722, Korea

⁷Theory division, Los Alamos National Laboratory, Los Alamos, New Mexico 87545, USA

(Dated: March 1, 2022)

X-ray photon correlation spectroscopy (XPCS) enables us to study dynamics of antiferromagnets. Using coherent soft X-ray diffraction, we resonantly probe Mn and Co Bragg peaks in the frustrated magnetic chain compound $\text{Lu}_2\text{CoMnO}_6$ significantly below the Néel temperature. Bragg peaks of incommensurate order slide towards commensurate ‘up up down down’ order with decreasing temperature. Antiferromagnetic inhomogeneities produce speckle within the Bragg peaks, whose dynamics are probed by XPCS and compared to the classic Axial Next-Nearest Neighbor Interaction model of frustration. The data supports a novel model prediction: with decreasing temperature the dynamics become faster.

Ferromagnetic (FM) domains have been studied for more than a century, revealing their key role in controlling the magnetic switching behavior and many other properties relevant to ferromagnetic applications. By contrast, antiferromagnetic (AFM) domains and other inhomogeneities have historically been challenging to image due to their lack of net magnetization. In the past few decades however, promising techniques have been developed based on X-rays [1–6] including X-ray photon correlation spectroscopy (XPCS). [7–10] AFM Bragg peaks are observed at the resonant edge of magnetic elements, allowing us to resolve speckle in the Bragg peak from coherent scattering off of AFM domains and inhomogeneities. The autocorrelation function of this speckle can be analyzed to extract statistical information. XPCS has led to e.g. observations of the dynamics of spin density waves in Cr [7] and of spin-helix phases in Dy [8, 9]. These techniques are timely to address the emergence of innovative ideas for the application of AFMs, such as exchange bias [11], spintronics [12–14] and multiferroics [15–18] as well as fundamental questions about the role of dynamic AFM in frustrated magnets. Thus far, XPCS studies of antiferromagnets have found that when the samples are cooled slightly below the Néel temperature $T < T_N$, the AFM dynamics become slow or freeze, as would be intuitively expected from thermal activation [7–9].

Here we focus on an AFM material with dynamics over an extended range of T , due to strong geometrical frustration. The inability of frustrated magnets to simultaneously satisfy all pairwise interactions leads to many nearly-degenerate states near the ground state, and thus enables inhomogeneities

in space and time. Frustration in AFM was theoretically proposed shortly after the proposal of AFM itself [19, 20]. However, to date, the basic dynamic predictions have been difficult to test directly. Thus, the recently-developed technique of XPCS tuned to the resonance of magnetic ions and the AFM Bragg peak is important to enable us to tackle the problem of AFM domain dynamics.

We study a long-standing problem in frustrated magnetism - the Axial Next-Nearest Neighbor Ising (ANNNI) model [21, 22]. In this model, nearest-neighbor FM interactions compete with next-nearest-neighbor AFM interactions along chains of Ising spins. This apparently simple model predicts complex behavior. As an ANNNI system is cooled below T_N , it passes through a theoretically infinite number of first order phase boundaries separating AFM phases with different commensurate (CM) or incommensurate (ICM) wavevectors, referred to as the ‘Devil’s staircase’ [23]. This large density of phases and phase transitions below T_N has interesting dynamic consequences, as we shall show both experimentally and theoretically below. At the lowest T , the ANNNI model predicts a CM wave vector such as ‘up up down down’ magnetic moment orientation along the chains. There have been previous XPCS investigations of e.g. frustrated magnets Dy and Cr that also show ICM order due to frustration between nearest and next-nearest neighbors, however they do not have Ising spins and thus they are not examples of the ANNNI model and dynamics were only observed in the immediate vicinity of T_N [7, 9].

We investigate the double perovskite compound

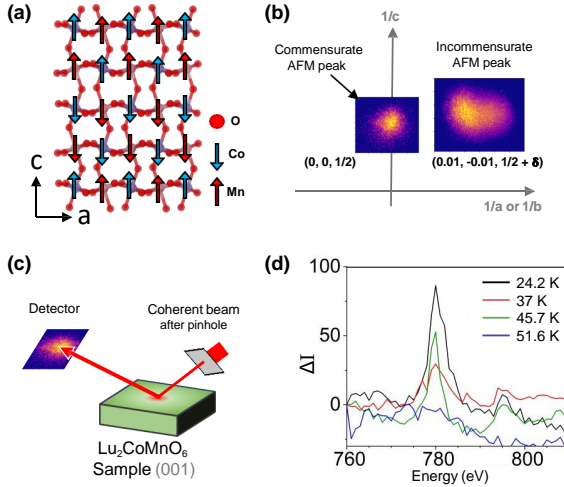


Figure 1. (a) Structure of $\text{Lu}_2\text{CoMnO}_6$ with spins, shown as arrows, with Lu atoms omitted. (b) Detected CM and ICM Bragg peaks, shown with their respective reciprocal space wavevector. (c) Experimental setup of resonant XPCS experiment, where the c -axis is normal to the illuminated face of the sample. (d) Energy spectrum for the ICM Bragg peak at the Co L_3 edge. Peak intensity was integrated over the detector area, with ΔI expressed as the relative change of the intensity at 780 eV vs. incident X-ray energy.

$\text{Lu}_2\text{CoMnO}_6$ [24–27]. Its physical properties, muon spin resonance (μSR) and neutron diffraction experiments have been previously interpreted in the context of the ANNNI model [28]. Co^{2+} and Mn^{4+} with $S = 3/2$ spins occupy oxygen cages, and the two magnetic ions alternate along the a , b , and c axes [24] with lattice spacing of $a = 5.1638(1)$ Å, $b = 5.5467(1)$ Å, $c = 7.4153(1)$ Å. A powder neutron diffraction study found that the magnetic state at 4 K consists of $\text{Co} \uparrow \text{Mn} \uparrow \text{Co} \downarrow \text{Mn} \downarrow$ configurations with both the spins and wave vector along the c axis, and a slight incommensuration with $\vec{k} \approx [0.0223(8), 0.0098(7), 0.5]$ (see Fig. 1(a)) [24]. Since the compound is multiferroic [24–27] previous studies used the magnetization and electric polarization to determine that this system has slow dynamics on hour time scales, as well as frequency dependence of these quantities in the kHz frequency range. These dynamics were observed between $T_N = 48$ K and $T_{\text{Hyst}} = 30 - 35$ K. Dynamics between ps and μs timescales were also uncovered by measuring μSR and neutron diffraction [28]. Below T_{Hyst} , hysteresis appeared in the magnetization and electric polarization suggesting that AFM and field-induced FM domains become pinned below this temperature by spin-lattice interactions [24, 27].

We performed XPCS measurements on mm-sized single crystals of $\text{Lu}_2\text{CoMnO}_6$ [26] at the Coherent Soft X-ray Scat-

tering (CSX, 23-ID-1) beamline at NSLS-II [10] during three different beam times. The crystals were polished on their (001) faces down to $0.3 \mu\text{m}$, and mounted with the (001) face upward on a copper sample holder with silver paint. Coherent X-rays passed through a $10 \mu\text{m}$ pinhole, then resonantly Bragg scattered off the Co or Mn ions in the geometry shown in Fig. 1. Each speckle pattern was recorded at a fixed T every 3.25 s for up to three hrs, after allowing for thermalization (approximately 1 hour). The dynamics of the speckle pattern, and thus the domain patterns which they encode, were analyzed by computing the autocorrelation function $g^{(2)}(\vec{q}, \tau)$ of the speckle intensity $I(\vec{q}, t)$: $g^{(2)}(\vec{q}, \tau) = \langle I(\vec{q}, t)I(\vec{q}, t + \tau) \rangle / \langle I(\vec{q}, t) \rangle^2$. Here, the intensities $I(\vec{q}, t)$ and $I(\vec{q}, t + \tau)$ are extracted for a particular momentum vector \vec{q} at times t and $t + \tau$, with τ being a delay time and angle brackets denoting time averaging.

We investigate the two satellite ICM Bragg peaks $\vec{k} = [\pm\delta, \mp\delta, 1/2 \mp \epsilon]$ and a CM Bragg peak $\vec{k} = [0, 0, 1/2]$, where the CM peak corresponds to the ‘up up down down’ ordering. δ and ϵ are in the range of 0.01 or lower and decrease with T [29]. Data was taken at Co and Mn edges for σ and π X-ray polarization, and a complete XPCS data set was taken at the Co edge with π polarization since it had the largest magnitude. The ICM wave vectors are slightly different than those found in polycrystalline neutron diffraction data [24], however they are more accurate since they are extracted from single crystals. They include incommensuration along the c -axis, which is a prediction of the ANNNI model.

We find that above T_{Hyst} (the region where physical properties have no hysteresis in T or magnetic field) the nominal CM $[0, 0, 1/2]$ Bragg peak has no resolvable energy dependence near the Co or Mn L_3 edges, showing that is not at a magnetic resonance. We conclude that it is dominated by the first harmonic of the X-ray beam diffracting off the $[0, 0, 1]$ lattice peak. However, below T_{Hyst} it acquires a strong resonance at the energy of the Co and Mn L_3 edges thus this Bragg peak becomes dominated by the $[0, 0, 1/2]$ magnetic peak. Meanwhile, the ICM peaks can be observed only at the Co and Mn L_3 edges at all $T < T_N$, both above and below T_{Hyst} , proving their magnetic character. There is a small T -dependence of δ and ϵ (shown in the S.I. [29]) such that the ICM peaks approaches the CM $\vec{k} = [0, 0, 1/2]$ position as T is lowered from T_N to T_{Hyst} , as predicted for the ANNNI model. The fact that the CM peak abruptly acquires a magnetic component below T_{Hyst} , may indicate that part of the sample evolves all the way to the CM order as T is lowered, while another part of the sample remains trapped in a state described by an ICM wavevector. The wave vectors of the CM and ICM peaks were reproducible at different locations on the sample, though the ICM peaks were not always visible.

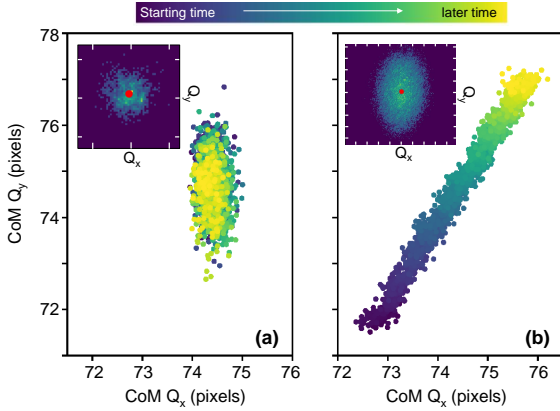


Figure 2. Center of Mass (CoM) of CM (a) and ICM (b) peaks at 35 K shown in detector pixels ($1 \text{ pixel} = 7 \times 10^{-5} \text{ \AA}^{-1}$). The color denotes relative position in time over 1.8 hrs. Insets show a full Bragg peak with red dot indicating CoM extracted from an Otsu thresholded detector image, and white hashmarks denoting 20 pixel intervals.

We also noted a significant drift in the magnetic ICM Bragg peak position over time for $T > T_{\text{Hyst}}$. This drift is shown in Fig 2 over a roughly 2 hour period, with a lack of drift in CM peak shown for comparison. Additional information is given in the S.I. [29]. Similar drifts have been observed in the ANNNI spin chain compound $\text{Ca}_3\text{Co}_2\text{O}_6$ [30, 31] and were attributed to the inability of the system to reach its stable ICM wave vector after a change in T due to very slow dynamics.

Figure 3 (a) and (b) shows the ICM peak at the Co edge at 778 eV, measured in a π configuration at $T = 35 \text{ K}$ and 24 K , just above and below $T_{\text{Hyst}} = 30 \text{ K}$. On the right are waterfall plots, showing an average over a vertical stripe through the center of the Bragg peak $1.4 \times 10^{-4} \text{ \AA}^{-1}$ wide (2 pixels) vs time. The ICM speckle pattern is relatively unchanged at 35 K over the 3 hours, whereas at 25 K the speckle shifts and decorrelates on a shorter timescale. This behavior was verified in several different beam times. Thus, at 35 K the ICM peak drifts but does not decorrelate, and at 25 K the ICM peak decorrelates but does not drift.

In Fig. 3 (c) and (d) the normalized intermediate scattering function $g^{(2)} - 1$ (the autocorrelation function between the signal at different times) is shown at $T = 25, 35$ and 55 K . The autocorrelation is normalized to the average of $g^{(2)} - 1$ within the first 30 s of integration, serving as a representative baseline. Exact regions of interest (ROIs) used in the calculation can be found in the S.I. [29] Since 55 K is above T_N , there is no Bragg peak for the ICM case. Autocorrelation functions for other sub-regions of the CM Bragg peak were unable to discern notably separate dynamics between the central and outer portions of the Bragg peak (see S.I. [29]).

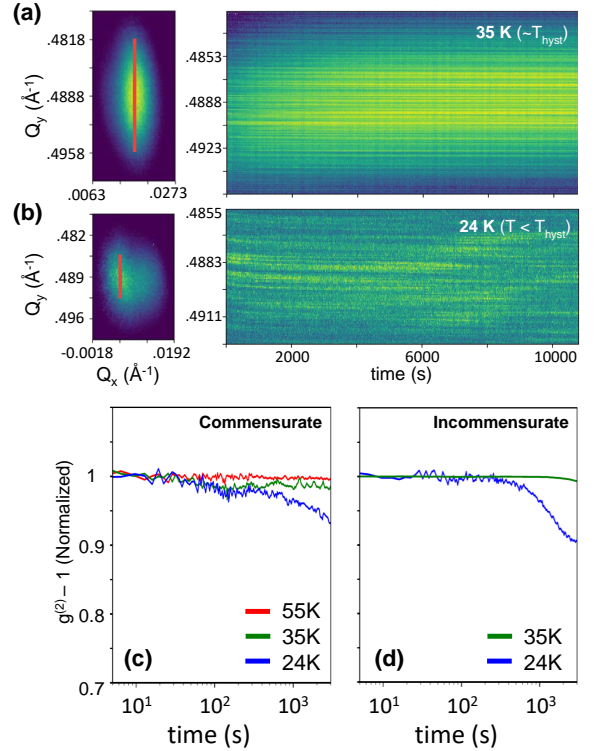


Figure 3. a) (Right) Waterfall plot showing Cross section of ICM Bragg peak at 35 K shown vs time, where cross section is integrated over the red lineout defined on the Left. b) Similar waterfall plot for 24 K. c) Normalized autocorrelation function ($g^{(2)} - 1$) vs. time for the CM peak at $[0, 0, 1/2]$ and d) ICM peak at $[0.0087, -0.0042, 0.489]$ and $[0.0168, -0.006, 0.4888]$ at 35 K. All data is shown for the Co L_3 edge with π polarization.

Thus, by means of XPCS we measure that the speckle from domains in the purely magnetic ICM peaks at 25 K (below T_{Hyst}) decorrelate significantly more rapidly than at 35 K. While this observation is counterintuitive in general, since dynamics usually freeze at low T , it is in fact a prediction of the ANNNI model due to the presence of a Devil's staircase of 1^{st} order phase transitions. These dense 1^{st} order phase boundaries can lead to an effective pinning of ICM wavevectors and consequently slower magnetic dynamics. Below T_{Hyst} on the other hand, large stable magnetic domains form and the dynamic speckle behavior is produced by faster local fluctuations within each domain. In the following, we calculate the dynamics in an ANNNI Monte Carlo model.

Monte Carlo simulations of the dynamic behavior of the ANNNI model were performed to compare with the experimental data. We note that in $\text{Lu}_2\text{CoMnO}_6$ there are two magnetic ions instead of one which is a deviation from the clas-

sic single-ion ANNNI model. We perform simulations for the two-ion ANNNI model (here) and compare to the single-ion ANNNI model (S.I.) to confirm that the dynamics are similar.

The in-plane ordering wavevector is small, thus we assume a simple nearest-neighbor FM interaction in the $a - b$ plane. The spin Hamiltonian is expressed as:

$$\mathcal{H} = -J_1 \sum_{NN} \sigma_i S_j^z - J_2 \sum_{NNN} \sigma_i \sigma_j - J_2' \sum_{NNN} \mathbf{S}_i \cdot \mathbf{S}_j - A \sum_i (S_i^z)^2,$$

where $\sigma_j = \pm 1$ is the Co^{2+} Ising spin and $|\mathbf{S}_j| = 1$ is the Mn^{4+} Heisenberg spin with an easy axis anisotropy, $A > 0$. \mathbf{S}_j and σ_j form two sublattices of the square lattice, as shown in Fig. 4 (a). $J_1 > 0$ is the nearest-neighbor (NN) FM interaction, and $J_2 < 0$ and $J_2' < 0$ are the next-nearest neighbor (NNN) AFM interaction along the c axis. We choose $J_2 = J_2' = -0.6J_1$ and $A = J_1$ to match the experimental T_N and T_{Hyst} . We employ a 2-D model corresponding to the $a - c$ plane of $\text{Lu}_2\text{CoMnO}_6$ and perform Monte Carlo simulations of \mathcal{H} with the standard Metropolis algorithm.

The calculated ordering wavevector Q vs. T is shown in Fig. 4(a). Because of the finite size effect, Q changes step-wise with T . There are peaks in the calculated specific heat when Q changes, which correspond to the 1st order phase transition between different Q states. The 1st order phase transition implies slow dynamics in the ICM phase. For increasing system size, Q changes quasi-continuously through many weak 1st order transitions. To capture the dynamics, we compute the autocorrelation function of the spin structure factor $S(Q, t) \equiv \langle M_z(Q, t) M_z(-Q, t) \rangle$, represented as:

$$A(t) = \int_0^\tau dt_1 (\mathbf{S}(t_1) - \bar{\mathbf{S}}) (\mathbf{S}(t + t_1) - \bar{\mathbf{S}}) / \int_0^\tau dt_1 (\mathbf{S}(t_1) - \bar{\mathbf{S}})^2,$$

where M_z is the z component of the magnetization at wavevector Q and $\langle \dots \rangle$ denotes thermal average. Here t is the Monte Carlo time and τ is the total simulation time, and $\bar{\mathbf{S}}$ is the mean value of $\mathbf{S}(Q, t)$. The results, displayed in Fig. 4(b), show that the dynamics for T between T_N and T_{Hyst} are extremely slow, slower than the region below T_{Hyst} . The correlation time is particular long at the first order phase transition point.

The simulations of the dynamics are qualitatively consistent with the XPCS results. The theory and experiment both show ‘inverted’ dynamics, where the speckle decorrelates faster below T_{Hyst} than above it.

In conclusion, we observe dynamics of speckle in CM and ICM peaks over a very broad range of temperature down to a quarter of T_N , and these dynamics are inverted in temperature from ordinary magnets - we observe fast dynamics at low T and slow dynamics at high T . We employ Monte Carlo simulations to show that these unusual dynamics are predicted by the

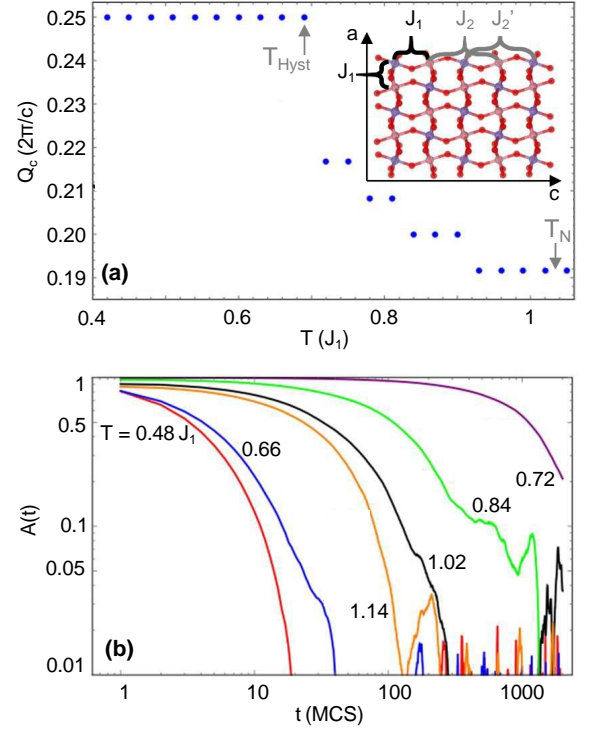


Figure 4. (a) Monte Carlo simulations of the ICM AFM wavevector Q vs T , obtained by slowly cooling to $T = 0$ and then heating. Inset shows the magnetic model with nearest and next-nearest neighbor magnetic interactions. (b) Calculated spin autocorrelation function $A(t)$ at fixed $Q = 0.25 \times 2\pi/c$ vs time for varying T . Time (t) is shown in units of Monte Carlo sweep (MCS).

ANNNI model. Above T_{Hyst} the ANNNI model predicts many (theoretically infinite) first order phase transitions occurring at closely-spaced temperatures whose domain boundaries pin the ICM wave vectors, creating slow dynamics. This manifests as slow decorrelation in the speckle measured by XPCS as well as drifting ICM wave vectors that do not stabilize within three hrs after changes in T . On the other hand, below T_{Hyst} the system has stable pinned domains and so the dynamics are dominated by fast fluctuations within each domain.

ACKNOWLEDGEMENTS

We are grateful to Ashish Tripathi, Benjamin Pound, Sha-linee Chikara for helpful discussions and experimental aid. Scientific work was supported by the LDRD program at LANL. This research utilized beamline 23-ID-1 of the National Synchrotron Light Source II, a U.S. DOE Office of Science User Facility operated for the DOE Office of Sci-

ence by Brookhaven National Laboratory under Contract No. DE-SC0012704; as well as the facilities of the Center for Integrated Nanotechnologies, an Office of Science User Facility operated for the U.S. DOE Office of Science by LANL; and finally the facilities of the National High Magnetic Field Lab, funded by the U.S. National Science Foundation through Cooperative Grant No. DMR-1157490, the State of Florida, and the U.S. DOE. Sample growth efforts at Yonsei University were supported by the National Research Foundation of Korea Grants NRF-2017R1A5A1014862 (SRC program: vdWMRC center, NRF-2018R1C1B6006859, and NRF-2019R1A2C2002601).

* These authors contributed equally

† Now at: Idaho National Laboratory, Idaho Falls, Idaho

- [1] M. Schwickert, G. Guo, M. Tomaz, W. O'Brien, and G. Harp, *Phys. Rev. B* **58**, R4289 (1998).
- [2] J. Kortright, D. Awschalom, J. Stöhr, S. Bader, Y. Idzerda, S. Parkin, I. K. Schuller, and H.-C. Siegmann, *J. Magn. Magn. Mat.* **207**, 7 (1999).
- [3] F. Nolting, A. Scholl, and J. Stöhr, *Nature* **405**, 767 (2000).
- [4] J. Stöhr and H. C. Siegmann, *Magnetism: From Fundamentals to Nanoscale Dynamics*, Vol. 1 (SPRINGER, 2006).
- [5] T. Zhao, A. Scholl, F. Zavaliche, K. Lee, M. Barry, A. Doran, M. P. Cruz, Y. H. Chu, C. Ederer, N. A. Spaldin, R. R. Das, D. M. Kim, S. H. Baek, C. B. Eom, and R. Ramesh, *Nature Mat.* **5**, 823 (2006).
- [6] M. G. Kim, H. Miao, B. Gao, S.-W. Cheong, C. Mazzoli, A. Barbour, W. Hu, S. B. Wilkins, I. K. Robinson, M. P. M. Dean, and V. Kiryukhin, *Nature Comm.* **9**, 5013 (2018).
- [7] O. G. Shpyrko, E. D. Isaacs, J. M. Logan, Y. Feng, G. Aeppli, R. Jaramillo, H. C. Kim, T. F. Rosenbaum, P. Zschack, M. Sprung, S. Narayanan, and A. R. Sandy, *Nature* **447**, 68 (2006).
- [8] S. Konings, C. Schüßler-Langeheine, H. Ott, E. Weschke, E. Schierle, H. Zabel, and J. B. Goedkoop, *Phys. Rev. Lett.* **106**, 077402 (2011).
- [9] S.-W. Chen, H. Guo, K. A. Seu, K. Dumesnil, S. Roy, and S. K. Sinha, *Phys. Rev. Lett.* **110**, 217201 (2013).
- [10] X. M. Chen, V. Thampy, C. Mazzoli, A. M. Barbour, H. Miao, G. D. Gu, Y. Cao, J. M. Tranquada, M. P. M. Dean, and S. B. Wilkins, *Phys. Rev. Lett.* **117**, 167001 (2016).
- [11] J. Nogues and I. Schuller, *J. Magn. Magn. Materials* **192**, 203 (1999).
- [12] S. D. Bader and S. S. P. Parkin, *Annu. Rev. Condens. Matter Phys.* **1**, 71 (2010).
- [13] J. Barker and O. A. Tretiakov, *Physical review letters* **116**, 147203 (2016).
- [14] I. Gross, W. Akhtar, V. Garcia, L. J. Martínez, S. Chouaieb, K. Garcia, C. Carrétéro, A. Barthélémy, P. Appel, P. Maletinsky, J. V. Kim, J. Y. Chauleau, N. Jaouen, M. Viret, M. Bibes, S. Fusil, and V. Jacques, *Nature* **549**, 252 (2017).
- [15] R. Ramesh and N. A. Spaldin, *Nat. Mater.* **6**, 21 (2007).
- [16] Y. H. Chu, L. W. Martin, M. B. Holcomb, M. Gajek, S.-J. Han, Q. He, N. Balke, C.-H. Yang, D. Lee, W. Hu, Q. Zhan, P.-L. Yang, A. Fraile-Rodríguez, A. Scholl, S. X. Wang, and R. Ramesh, *Nat. Mater.* **7**, 478 (2008).
- [17] X. Marti, I. Fina, C. Frontera, J. Liu, P. Wadley, Q. He, R. J. Paull, J. D. Clarkson, J. Kudrnovský, I. Turek, J. Kuneš, D. Yi, J. H. Chu, C. T. Nelson, L. You, E. Arenholz, S. Salahuddin, J. Fontcuberta, T. Jungwirth, and R. Ramesh, *Nature Materials* **13**, 367 (2014).
- [18] W. Legrand, D. Maccariello, F. Ajejas, S. Collin, A. Vecchiola, K. Bouzehouane, N. Reyren, V. Cros, and A. Fert, *Nature Materials* (2019), 10.1038/s41563-019-0468-3.
- [19] M. L. Néel, *Annales de Physique* **12**, 137 (1949).
- [20] G. H. Wannier, *Phys. Rev.* **79**, 357 (1950).
- [21] P. Bak, *Rep. Prog. Phys.* **45**, 587 (1982).
- [22] W. Selke, *Physics Reports* **170**, 213 (1988).
- [23] P. Bak and M. H. Jensen, *J. Phys. C* **13**, L881 (1980).
- [24] S. Yáñez-Vilar, E. D. Mun, V. S. Zapf, B. G. Ueland, J. S. Gardner, J. D. Thompson, J. Singleton, M. Sánchez-Andújar, J. Mira, N. Biskup, M. A. Señarís-Rodríguez, and C. D. Batista, *Phys. Rev. B* **84**, 134427 (2011).
- [25] N. Lee, H. Y. Choi, Y. J. Jo, M. S. Seo, S. Y. Park, and Y. J. Choi, *Applied Physics Letters* **104**, 112907 (2014).
- [26] S. Chikara, J. Singleton, J. Bowlan, D. A. Yarotski, N. Lee, H. Y. Choi, Y. J. Choi, and V. S. Zapf, *Phys. Rev. B* **93**, 180405 (2016).
- [27] H. Y. Choi, J. Y. Moon, J. H. Kim, Y. J. Choi, and N. Lee, *Crystals* **7** (2017).
- [28] V. S. Zapf, B. G. Ueland, M. Laver, M. Lonsky, M. Pohlit, J. Müller, T. Lancaster, J. S. Möller, S. J. Blundell, J. Singleton, J. Mira, S. Yáñez Vilar, and M. A. Señarís Rodríguez, *Phys. Rev. B* **93**, 134431 (2016).
- [29] Supplementary Information at [URL will be inserted by publisher] contains additional XPCS data and analysis, and discussion of some details.
- [30] T. Moyoshi, R. Takahashi, and K. Motoya, *J. Phys.: Conf. Series* **273**, 012125 (2011).
- [31] S. Agrestini, C. L. Fleck, L. C. Chapon, C. Mazzoli, A. Bombardi, M. R. Lees, and O. A. Petrenko, *Phys. Rev. Lett.* **106**, 197204 (2011).